OXFORD

Human Molecular Genetics, 2015, Vol. 24, No. 25 7390–7405

doi: 10.1093/hmg/ddv439
Advance Access Publication Date: 19 October 2015
Original Article

ORIGINAL ARTICLE

Amyotrophic lateral sclerosis and denervation alter sphingolipids and up-regulate glucosylceramide synthase

Alexandre Henriques[1,2], Vincent Croixmarie[3], David A. Priestman[4], Angela Rosenbohm[5], Sylvie Dirrig-Grosch[1,2], Eleonora D'Ambra[1,2], Mylene Huebecker[4], Ghulam Hussain[1,2,6], Claire Boursier-Neyret[3], Andoni Echaniz-Laguna[1,2,7], Albert C. Ludolph[5], Frances M. Platt[4], Bernard Walther[3], Michael Spedding[8,9], Jean-Philippe Loeffler[1,2] and Jose-Luis Gonzalez De Aguilar[1,2,*]

[1]Université de Strasbourg, UMR_S 1118, Strasbourg, France, [2]INSERM, U1118, Mécanismes Centraux et Péripheriques de la Neurodégénérescence, Strasbourg, France, [3]Technologie Servier, Orleans, France, [4]Department of Pharmacology, University of Oxford, Oxford, UK, [5]Department of Neurology, University of Ulm, Ulm, Germany, [6]Department of Physiology, GC University, Faisalabad, Pakistan, [7]Hôpitaux Universitaires, Département de Neurologie, Strasbourg, France, [8]Les Laboratoires Servier, Suresnes, France and [9]Spedding Research Solutions SARL, Le Vesinet, France

*To whom correspondence should be addressed at: Université de Strasbourg, INSERM U1118, Mécanismes Centraux et Péripheriques de la Neurodégénérescence, Faculté de Médecine, Bâtiment 3, Etage 8, 11 rue Humann, F-67085 Strasbourg, France. Tel: +33 368853091; Fax: +33 368853065; Email: gonzalez@unistra.fr

Abstract

Amyotrophic lateral sclerosis (ALS) is a fatal adult-onset disease characterized by upper and lower motor neuron degeneration, muscle wasting and paralysis. Growing evidence suggests a link between changes in lipid metabolism and ALS. Here, we used UPLC/TOF-MS to survey the lipidome in SOD1(G86R) mice, a model of ALS. Significant changes in lipid expression were evident in spinal cord and skeletal muscle before overt neuropathology. *In silico* analysis also revealed appreciable changes in sphingolipids including ceramides and glucosylceramides (GlcCer). HPLC analysis showed increased amounts of GlcCer and downstream glycosphingolipids (GSLs) in SOD1(G86R) muscle compared with wild-type littermates. Glucosylceramide synthase (GCS), the enzyme responsible for GlcCer biosynthesis, was up-regulated in muscle of SOD1(G86R) mice and ALS patients, and in muscle of wild-type mice after surgically induced denervation. Conversely, inhibition of GCS in wild-type mice, following transient peripheral nerve injury, reversed the overexpression of genes in muscle involved in oxidative metabolism and delayed motor recovery. GCS inhibition in SOD1(G86R) mice also affected the expression of metabolic genes and induced a loss of muscle strength and morphological deterioration of the motor endplates. These findings suggest that GSLs may play a critical role in ALS muscle pathology and could lead to the identification of new therapeutic targets.

Received: August 18, 2015. **Revised and Accepted:** October 12, 2015

Introduction

Amyotrophic lateral sclerosis (ALS) is a devastating neurological disorder characterized by the selective degeneration of upper motor neurons in the motor cortex and lower motor neurons in the brainstem and the spinal cord. ALS is essentially incurable. Clinical hallmarks include progressive muscle wasting, speech and swallowing difficulties, fasciculations, altered reflexes and spasticity. Death by respiratory complications usually occurs within 2–5 years of diagnosis. The disease usually appears between 40 and 70 years of age and affects ~1 in 50 000 people. About 90% of cases are sporadic, whereas the remaining 10% exhibit a Mendelian pattern of inheritance, mainly in an autosomal dominant manner (1). As both sporadic and familial forms are clinically and pathologically undistinguishable, there are likely to be common pathogenic mechanisms. Gene mutations implicated in the pathogenesis of ALS are listed at http://alsod.iop.kcl.ac.uk/. In Caucasian people, mutations in the *sod1* gene, which encodes the free radical-scavenging enzyme Cu/Zn superoxide dismutase, account for ~20% of familial cases and 2–7% of sporadic cases (2,3). Transgenic mice with mutations in *sod1* are a well-characterized animal model of human ALS and have precipitous, age-related loss of motor neurons (4–6).

One complication of ALS is abnormal regulation of energy homeostasis (7–9). Overexpression of mutant SOD1 in mice induces a reduction in fat pad mass with increased rates of energy expenditure, before any sign of motor impairment (10–12). In ALS patients, several indices of dyslipidemia, including a high LDL/HDL cholesterol ratio, elevated total cholesterol or triglycerides and a high palmitoleic-to-palmitic fatty acid ratio, are associated with better prognosis (13–17). Other classes of lipids, such as sphingomyelin, ceramides, cholesterol esters and omega-3 polyunsaturated fatty acids, are altered in the spinal cord of ALS patients and mutant SOD1 mice, although the effects of these alterations in the central nervous system deserve further investigation (18,19). In all, these findings strongly suggest intimate relationships between changes in lipid metabolism and ALS pathology.

Recent metabolomic approaches have identified a number of metabolites as being involved in ALS by as yet unclear mechanisms (20–26). In this study, we extracted lipids from spinal cord and skeletal muscle of mutant SOD1 mice at pre-symptomatic and symptomatic stages. Three thousand lipid species were compared using ultra-performance liquid chromatography coupled to time-of-flight mass spectrometry (UPLC/TOF-MS). This technique allows highly selective separation of molecular species, together with values for their molecular masses (27). *In silico* analysis of these data mainly revealed significant pre-symptomatic alterations in sphingolipids. We therefore investigated glucosylceramide synthase (GCS, also referred to as UDP-glucose ceramide glucosyltransferase), an essential Golgi transmembrane enzyme responsible for the synthesis of glucosylceramides (GlcCer), which is the first step in the pathway of glycosphingolipid (GSL) biosynthesis (28). We show that there are changes in GCS and thereby GlcCer and some downstream GSLs in ALS muscle pathology, and in response to surgically induced muscle denervation. These findings could lead to the identification of new therapeutic targets.

Results

Lipid composition is altered in spinal cord and muscle of pre-symptomatic SOD1(G86R) mice

We studied differences in the lipidomes of wild-type (WT) and SOD1(G86R) mice at pre-symptomatic and symptomatic ages (Supplementary Material, Fig. S1). Unsupervised principal component analysis (PCA) of spinal cord and muscle samples revealed two clusters of individuals, corresponding to WT and SOD1(G86R) mice, respectively, that were clearly distinguishable even at the pre-symptomatic stage. We also performed partial least-squares discriminant analysis, which is a supervised alternative to differentiate between experimental groups. This analysis revealed lipid changes in spinal cord and muscle, which significantly distinguished SOD1(G86R) mice from WT littermates at the pre-symptomatic stage (Fig. 1). Very similar results were obtained with samples from symptomatic mice (Supplementary Material, Fig. S2). In spinal cord of pre-symptomatic and symptomatic mice, most lipids, which were affected, were decreased. In contrast, most of the lipids with significant changes in muscle of SOD1(G86R) mice were increased (Table 1).

Sphingolipids are affected in spinal cord and muscle of SOD1(G86R) mice

To further investigate the changes in the lipidome of SOD1(G86R) mice, we attributed hypothesis-based identifications to the significantly deregulated lipid species, according to their atomic masses in the HMDB database (29). Major changes in three lipid families were evident in the SOD1(G86R) lipidome (Fig. 2 and Supplementary Material, Fig. S3). Levels of most phospholipids and sphingolipids were decreased in spinal cord of pre-symptomatic and symptomatic mice compared with WT littermates. In contrast, levels of many of these lipids were increased in muscle at both stages. The majority of triglyceride species were reduced in muscle and, to a lesser extent, spinal cord of symptomatic mice compared with WT littermates, some even being entirely depleted. Triglycerides were also markedly depleted in plasma samples in these mice (data not shown), indicating the considerable lipid mobilization during the course of the disease (10). We obtained comparable patterns of expression when we used the METLIN database for the identification of metabolites (30) (Supplementary Material, Fig. S4). Next, we analyzed our data with ConsensusPathDB to decipher metabolic pathways of potential interest (31). This analysis revealed that changes in sphingolipid metabolism showed the highest statistical significance in the set of differentially regulated lipids in spinal cord (Supplementary Material, Table S1) and muscle (Supplementary Material, Table S2) of SOD1(G86R) mice. Several specific metabolites in this pathway appeared dysregulated: ceramide, dihydroceramide, dihydrosphingosine-1-phosphate, GlcCer, sphingomyelin and sphingosine (Supplementary Material, Fig. S5).

Glccer and GCS expression are up-regulated in muscle of SOD1(G86R) mice

Following the analysis described earlier, we also took advantage of our previously published transcriptome of muscle in SOD1 (G86R) mice (32). We performed a joint enrichment analysis of transcriptomics and lipidomics data using the IMPaLA web interface (33). This analysis revealed that the metabolism of sphingolipids, including ceramide and GlcCer, was among the most significantly over-represented pathways linked to the differential expression of GCS (Supplementary Material, Table S3), which is the enzyme responsible for the conversion of ceramides into GlcCer (28). As there is no available transcriptome database of spinal cord in SOD1(G86R) mice, we could not perform a similar analysis in this tissue. Based on these findings, we focused on GlcCer, because it is the precursor for all the more complex GSLs with important biological functions (34,35). HPLC analysis

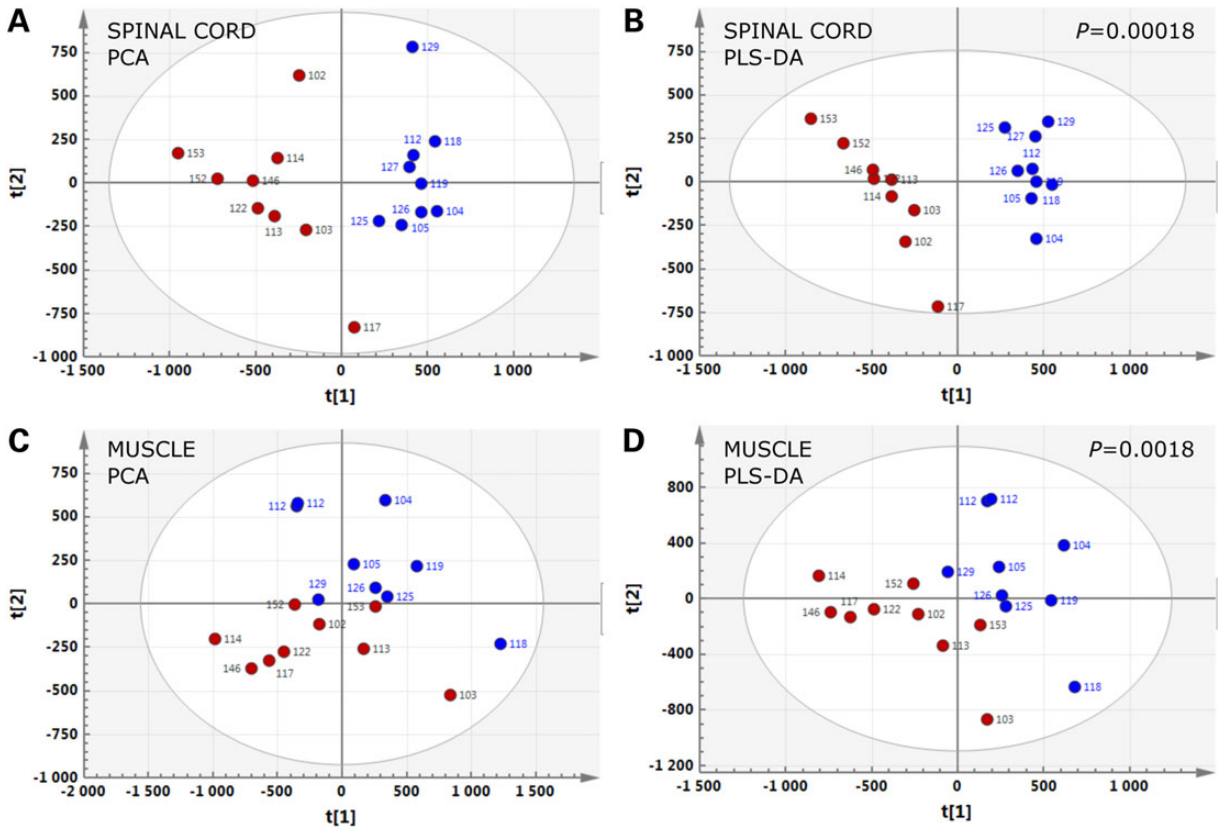

Figure 1. Lipidomic signatures in spinal cord and muscle of SOD1(G86R) mice. PCA (**A** and **C**) and PLS-DA (**B** and **D**) score plots showing the spatial distribution of SOD1 (G86R) mice at the pre-symptomatic stage (blue circles, $n = 9$) and WT littermates (red circles, $n = 9$), according to the lipidomic profiles of spinal cord (**A** and **B**) and muscle (**C** and **D**).

Table 1. Changes in lipid species in SOD1(G86R) mice

Stage	Spinal cord		Muscle	
A				
Pre-symptomatic	78	48%	76	26%
Pre-symptomatic and symptomatic	37	23%	69	24%
Symptomatic	46	29%	147	50%
Lipid species with significant changes	161		292	
Detected lipid species	1599		1518	

Stage	Regulation	Spinal cord		Muscle	
B					
Pre-symptomatic	Down	96	84%	8	6%
	Up	19	16%	137	94%
	Σ	115		145	
Symptomatic	Down	64	77%	81	38%
	Up	19	23%	135	62%
	Σ	83		216	

Specific changes between SOD1(G86R) and WT mice were identified using a multivariate PLS-DA model. A SOD1(G86R)-to-WT ratio was considered significant when the corresponding correlation coefficient in the S-plot built after the model was less than or equal to –0.7 (for down-regulated species) or greater than or equal to +0.7 (for up-regulated species). A shows the number of total changes observed in pre-symptomatic and symptomatic mice whereas B shows their classification into down- and up-regulated subsets (see Supplementary Fig. 1 and Statistical Analysis section for more details).

revealed a comparable age-related decline in the total amount of GlcCer in spinal cord of both SOD1(G86R) and WT mice (Fig. 3A). In contrast, a significant up-regulation of GM1a, the major ganglioside in the central nervous system, was observed in SOD1 (G86R) mice at the symptomatic stage compared with WT littermates (Fig. 3B). There was also a significant increase in GlcCer in muscle of symptomatic SOD1(G86R) mice (Fig. 3D). Concomitantly, levels of several gangliosides of the a-series, including GM3 and GM2, were significantly increased in this tissue (Fig. 3E). To investigate the reason for altered GlcCer levels, we measured GCS expression. GCS mRNA levels were significantly increased in muscle at both pre-symptomatic and symptomatic stages in SOD1(G86R) mice compared with WT littermates (Fig. 3F), but no differences were observed in spinal cord (Fig. 3C). Muscle GCS expression at 60 days of age, an earlier pre-symptomatic time point, was similar in SOD1(G86R) and WT mice (data not shown). Therefore, the up-regulation of GCS observed at 75 days of age can be considered as an early event preceding the onset of overt motor disease. To support these findings, we performed western blot analyses with actin or total protein content as an internal reference. In both cases, GCS protein amount was increased at the pre-symptomatic stage in SOD1(G86R) mice. This increase was similarly observed in symptomatic mice (Fig. 3G), although it was not noticeable after total protein normalization (data not shown). To gain further insight, muscle GCS expression was confirmed by immunohistological analysis of muscles from WT and SOD1(G86R) mice. We showed increased punctate GCS staining, frequently located at the border of myofibers (Fig. 3H),

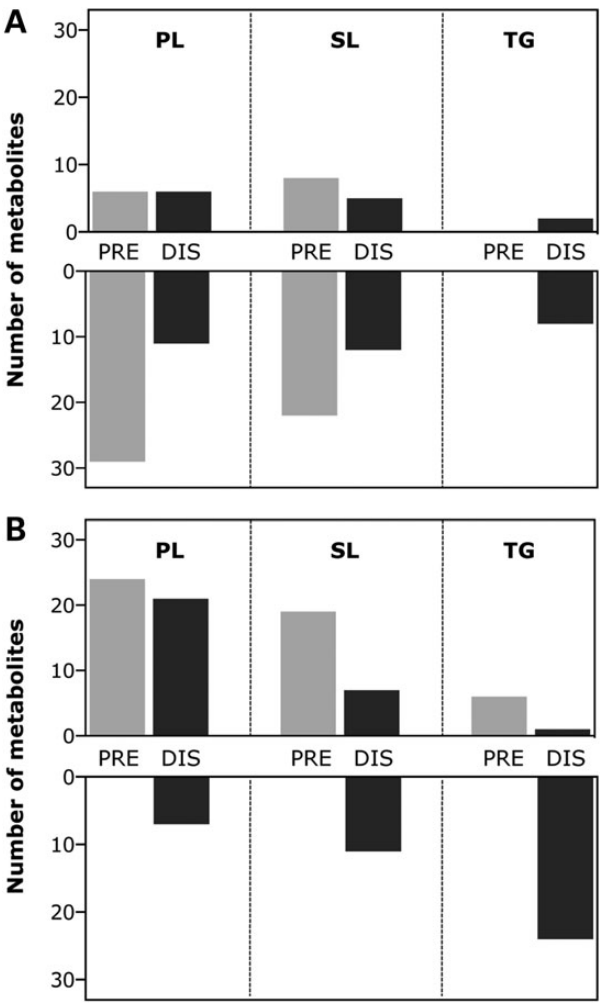

Figure 2. Major changes in three lipid families in spinal cord and muscle of SOD1 (G86R) mice. Distribution of differentially regulated phospholipid (PL), sphingolipid (SL) and triglyceride (TG) species in spinal cord (**A**) and muscle (**B**) of pre-symptomatic (PRE, light-colored bars, $n = 9$) and symptomatic (DIS, dark-colored bars, $n = 9$) SOD1(G86R) mice compared with WT littermates. Up- or down-regulated metabolites in each tissue are indicated in upper and lower panels, respectively.

compatible with the reorganization of Golgi complex in denervated muscle (36). This pattern of staining was specifically observed in myofibers exhibiting less cross-sectional area and more metabolic oxidative capacity, as assessed by an increase in the presence of mitochondrial succinate dehydrogenase (SDH) (Fig. 3I).

GCS expression is up-regulated in atrophic TDP-43-positive myofibers in ALS patients

Increased expression of GCS was also apparent in muscle of ALS patients compared with that of control subjects (Fig. 4A). This was confirmed by histological analysis of human muscle biopsies (Table 2). GCS appeared in the form of highly immunoreactive cytoplasmic inclusions usually located in the center of myofibers (Fig. 4B). These inclusions were more frequent in fibers with reduced cross-sectional area and, in many cases, with denervation-induced angulated morphology (Fig. 4C and D). Such a pattern of protein aggregation prompted us to investigate Tar-DNA binding protein-43 (TDP-43), because its abnormal accumulation in cytoplasmic inclusions is a pathological hallmark seen in the central nervous system in patients with frontotemporal lobar degeneration and ALS as well as in the muscles of patients with sporadic inclusion body myositis and its rare hereditary form presenting with Paget's disease of the bone and frontotemporal dementia (37–39). We showed that GCS co-localized with TDP-43 within the same inclusions in affected myofibers (Fig. 4E), which extends TDP-43 proteinopathy to ALS muscle and reveals GCS to be a major component of the inclusions that characterize human ALS muscle pathology.

GCS expression and GlcCer are up-regulated in response to surgically induced muscle denervation

To understand GCS up-regulation in muscle during ALS, we investigated the response of GCS to peripheral nerve injury in WT mice, as a way of mimicking ALS-like muscle denervation. Crushing the sciatic nerve for a few seconds is used as a model of hind limb denervation. This is followed by subsequent recovery owing to reinnervation in about 10 days. In contrast, axotomy, cutting and removing several millimeters of the sciatic nerve, causes denervation that persists for several weeks in WT mice. Muscle expression of the acetylcholine receptor alpha subunit (AChR-α) was strongly stimulated 3 days after crush injury in WT mice, at levels comparable to those found after 15 days following axotomy. This stimulatory effect was reduced by half, 15 days following the crush injury, when mice already exhibit signs of motor function recovery (Fig. 5A). Expression of the acetylcholine receptor epsilon subunit (AChR-ε) was significantly down-regulated 3 days following the crush injury and 15 days following axotomy, but expression was fully restored 15 days following crush (Fig. 5B). The decreased expression of AChR-α, together with the increased expression of AChR-ε, is interpreted as a sign of muscle re-innervation. Under these conditions, the pattern of expression of GCS (Fig. 5C), as well as that of RUNT-related transcription factor-1 (RUNX1) (Fig. 5D), a transcriptional activator of GCS (40), was similar to that of AChR-α. Western blot (Fig. 5E) and histological analysis (Fig. 5F) confirmed increased amounts of GCS in denervated muscle 3 days following crush injury. Furthermore, HPLC analysis revealed a significant increase in GlcCer, as well as GM3 and GM2 gangliosides, 10 days following crush injury (Fig. 5G). These findings reflect the observation in SOD1(G86R) mice and provide compelling evidence of the stimulatory effect of denervation on GlcCer and GSL accumulation.

GCS inhibition blocks the metabolic changes following muscle denervation and delays the recovery of motor function

In ALS, as well as in response to denervation, muscle atrophy is associated with changes in the metabolic phenotype of the fibers and modifications in their contractility and fatigability. These fibers undergo a shift from a fast-twitch to a slow-twitch type with more sustained activity and increased resistance to fatigue, characteristics that are typical of muscles with a high degree of oxidative, fatty acid metabolism (41–43). To determine the effects of inhibiting GCS enzymatic activity during muscle denervation, we treated WT mice, submitted to sciatic nerve crush, with daily intraperitoneal injections of the specific GCS inhibitor N-(5-adamantane-1-yl-methoxy-pentyl)-deoxynojirimycin (AMP-DNM) (44). AMP-DNM decreased muscle GlcCer content by 33% (Fig. 6A). Although this treatment did not influence the extent of muscle fiber atrophy 10 days following crush injury (Fig. 6B),

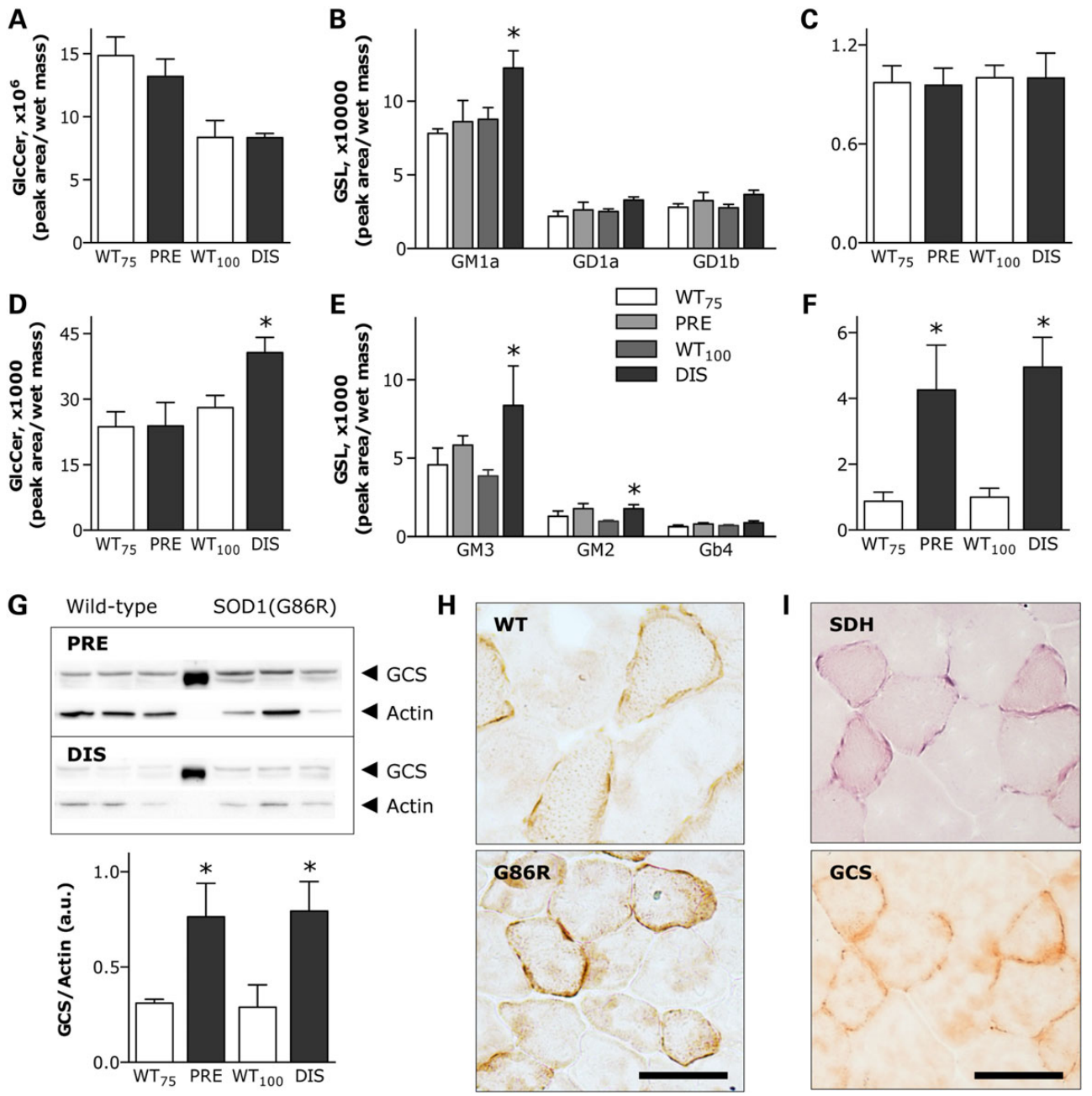

Figure 3. GlcCer/GSL metabolism in spinal cord and muscle of SOD1(G86R) mice. HPLC quantification of GlcCer and several GSLs in spinal cord (**A** and **B**) and muscle (**D** and **E**) of pre-symptomatic (PRE) and symptomatic (DIS) SOD1(G86R) mice compared with corresponding WT littermates. Only detected main peaks of gangliosides are shown in each tissue. *$P < 0.05$ versus corresponding WT, $n = 6$. Relative GCS mRNA levels in spinal cord (**C**) and muscle (**F**) of mice as in A. *$P < 0.05$ versus corresponding WT, $n = 6$–9. (**G**) GCS protein levels, as determined by western blot (upper panel), in muscle of mice as in A. Lower panel shows quantification of immunoblots using actin protein levels as internal reference. *$P < 0.05$ versus corresponding WT, $n = 3$. (**H**) Representative photomicrographs showing GCS immunostaining on cross-sections of WT and SOD1(G86R) muscle. Scale bar, 50 µm. (**I**) Representative photomicrographs showing mitochondrial SDH enzymatic activity and GCS immunostaining within the same myofibers on adjacent cross-sections. Scale bar, 50 µm.

it blocked the expression of several genes critical for promoting oxidative metabolism following denervation (Fig. 6C). In particular, AMP-DNM significantly reduced the expression of the transcription factors PGC1α and PPARα, master activators of mitochondriogenesis and lipid catabolism, respectively. At the same time, the expression of lipoprotein lipase (LPL), which hydrolyzes triglycerides, was significantly decreased. Finally, the expression of FAT/CD36, involved in fatty acid transport, and pyruvate dehydrogenase kinase-4 (PDK4), a promoter of β-oxidation of fatty acids, remained comparable to that of non-denervated muscle. This suggests a major effect on oxidative metabolism. The effect of GCS inhibition on neuromuscular function was also investigated after sciatic nerve crush. Ten days following crush injury, AMP-DNM did not affect overexpression of AChR-α in denervated muscle but significantly lowered expression of AChR-ε, when compared with levels observed in

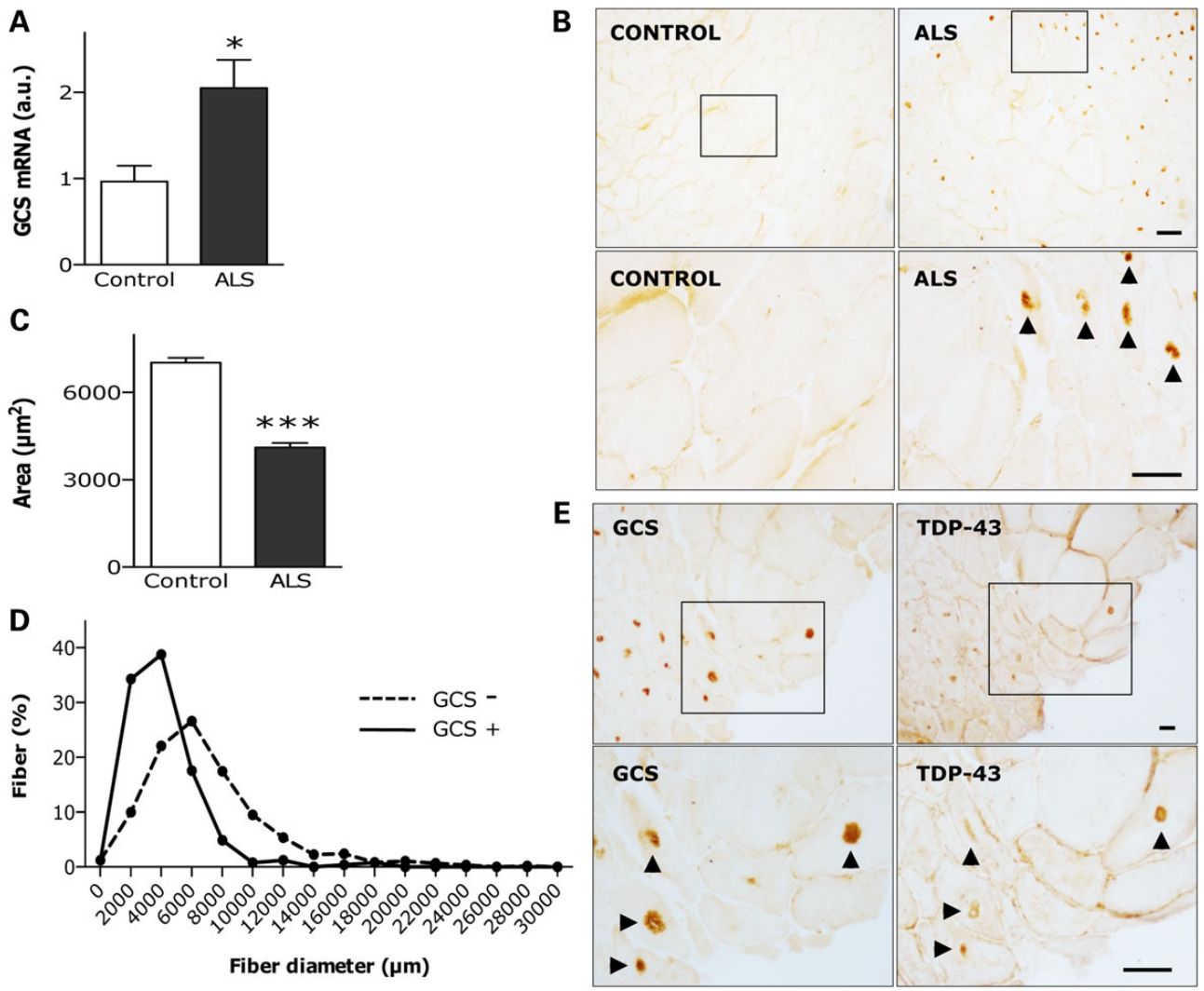

Figure 4. UGCG expression in human ALS muscle. (**A**) Relative GCS mRNA levels in deltoid muscle of 8 ALS patients and 12 control subjects. *$P < 0.05$. (**B**) Representative photomicrographs showing GCS immunostaining on cross-sections of vastus lateralis muscle of control (left panels) and ALS (right panels) individuals. Lower panels are magnifications of upper insets. Immunoreactive inclusions are indicated by arrow heads. Scale bar, 50 µm. Cross-sectional area of fibers (**C**), and distribution of fiber diameters (**D**) in sections as in B. Measurements were performed on 579 and 245 fibers from 4 control subjects and 6 ALS patients, respectively. ***$P < 0.001$. (**E**) Representative photomicrographs showing immunoperoxidase staining of GCS (left panels) and TDP-43 (right panels) on adjacent cross-sections of vastus lateralis muscle in ALS patients. Lower panels are magnifications of upper insets. Immunoreactive inclusions are indicated by arrow heads. Scale bars, 100 µm in upper panels, and 200 µm in lower panels.

Table 2. GCS immuno-positive inclusions in ALS patient muscle

Patient	Gender	Age	Diagnosis	Onset	ALSFRS-R	Muscle	Labeling
1	F	53	Fibromyalgia			Vastus lateralis	–
2	M	50	Fibromyalgia			Vastus lateralis	–
3	M	70	Fibromyalgia			Vastus lateralis	–
4	M	29	Fibromyalgia			Deltoid	–
1	M	56	ALS	Spinal	41	Vastus lateralis	++
2	M	70	ALS	Spinal	46	Vastus lateralis	–
3	M	73	ALS	Spinal	36	Vastus lateralis	+/–
4	M	82	ALS	Spinal	44	Gastrocnemius	++
5	M	60	ALS	Spinal	41	Vastus lateralis	+/–
6	M	70	ALS	Bulbar	37	Quadriceps	++

The presence of GCS immuno-positive inclusions was estimated as follows: score (–) was attributed to muscles with fibers deprived of inclusions, score (+/–) corresponded to muscles with small groups of fibers containing inclusions, and score (++) was attributed to muscles with many fibers containing inclusions. ALSFRS-R, revised ALS functional rating scale.

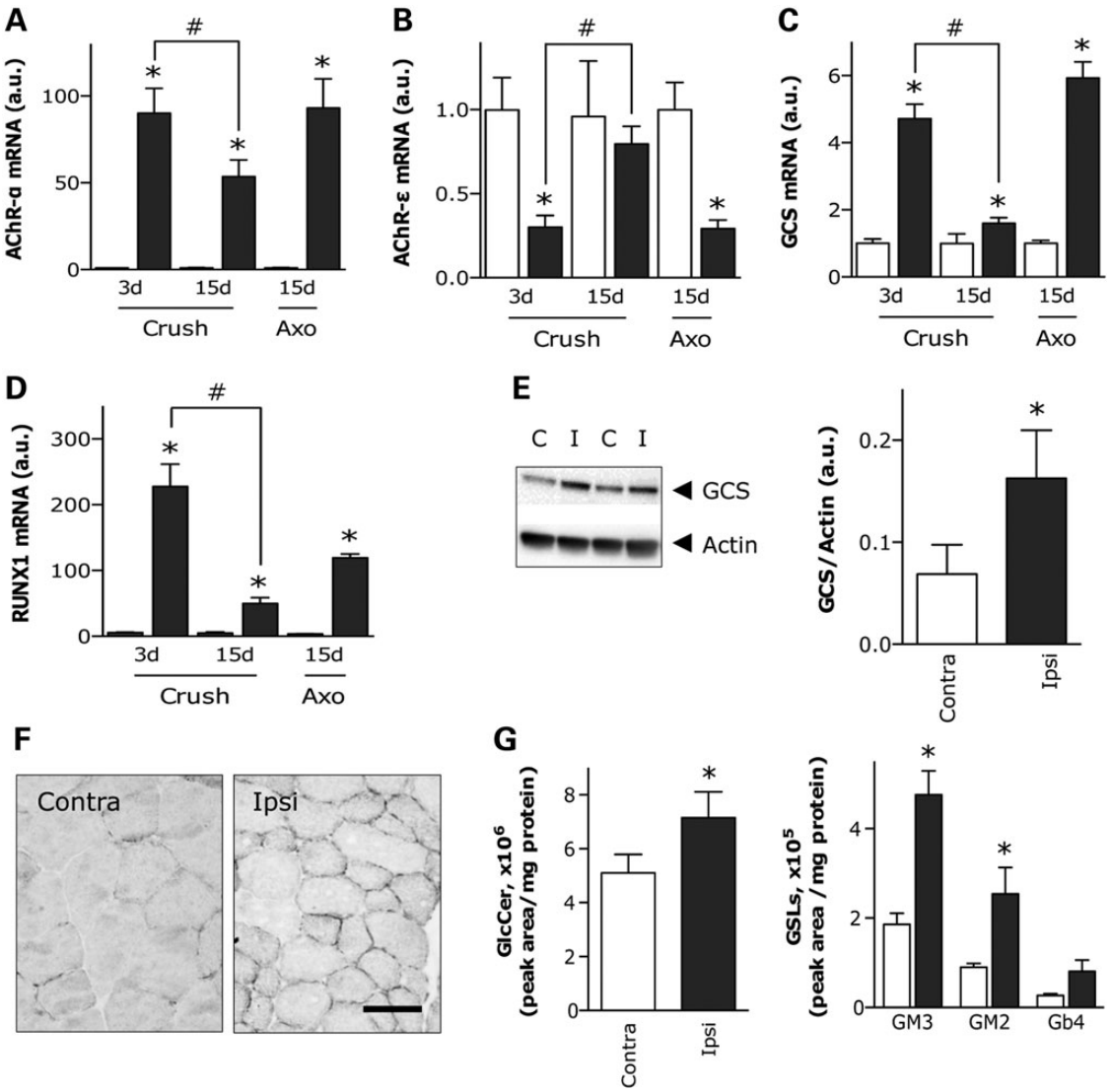

Figure 5. GCS expression in denervated muscle of WT mice. Relative mRNA levels of AChR-α (**A**), AChR-ε (**B**), GCS (**C**) and RUNX1 (**D**) in muscle of WT mice submitted to sciatic nerve crush or axotomy (Axo). Muscles were processed at the indicated days post-lesion. Ipsilateral muscles (red bars) were compared with contralateral muscles (white bars) in the same animal. *$P < 0.05$ versus corresponding contralateral muscle, #$P < 0.05$ versus preceding time point following nerve crush, $n = 5$–7. (**E**) GCS protein levels, as determined by western blot (a representative blot is shown in the left panel), in muscle of WT mice submitted to nerve crush as in A. Right panel shows quantification of immunoblots using actin protein levels as internal reference. *$P < 0.05$, $n = 8$. (**F**) Representative photomicrographs showing GCS immunostaining on cross-sections of contralateral and ipsilateral muscle as in A. Scale bar, 50 µm. (**G**) HPLC quantification of GlcCer (left panel) and several GSLs (right panel) in muscle of WT mice submitted to sciatic nerve crush as in A. Only detected main peaks of gangliosides are shown. *$P < 0.05$ versus corresponding contralateral muscle, $n = 7$–8.

denervated, untreated WT mice (Fig. 7A). Histological analysis of neuromuscular junctions in treated WT mice revealed that AMP-DNM significantly reduced the number of innervated synapses (Fig. 7B and C), which is interpreted as a delay in the process of axonal regeneration after crush. As a result, abnormal electromyographic episodes reflecting neurogenic denervation were more frequent and intense in AMP-DNM-treated mice (Fig. 7D). To monitor motor function recovery during reinnervation, we measured hind limb grip strength and found that its restoration was slower in treated WT mice than that in untreated littermates (Fig. 7E). In addition, the time to onset of toe spreading, considered as an index of reinnervation (45), was delayed in AMP-DNM-treated WT mice (median of 8 days), as compared with untreated WT mice (median of 3 days) (Fig. 7F). In all, these findings are consistent with a delayed regenerative capacity and strongly suggest a critical role for GCS in the response of muscle to denervation.

GCS inhibition alters neuromuscular junction integrity and modifies the expression of metabolic genes in muscle of SOD1(G86R) mice

Considering the detrimental effect of the inhibition of GCS on motor axis regeneration, we hypothesized that loss of enzymatic activity would predispose SOD1(G86R) mice to develop the disease phenotype earlier. To test this hypothesis, we treated SOD1(G86R) mice with AMP-DNM for 10 days, starting at the pre-symptomatic stage. We did not observe behavioral signs of disease onset, such as impaired locomotion or abnormal hind limb extension reflexes. However, we found that SOD1(G86R)

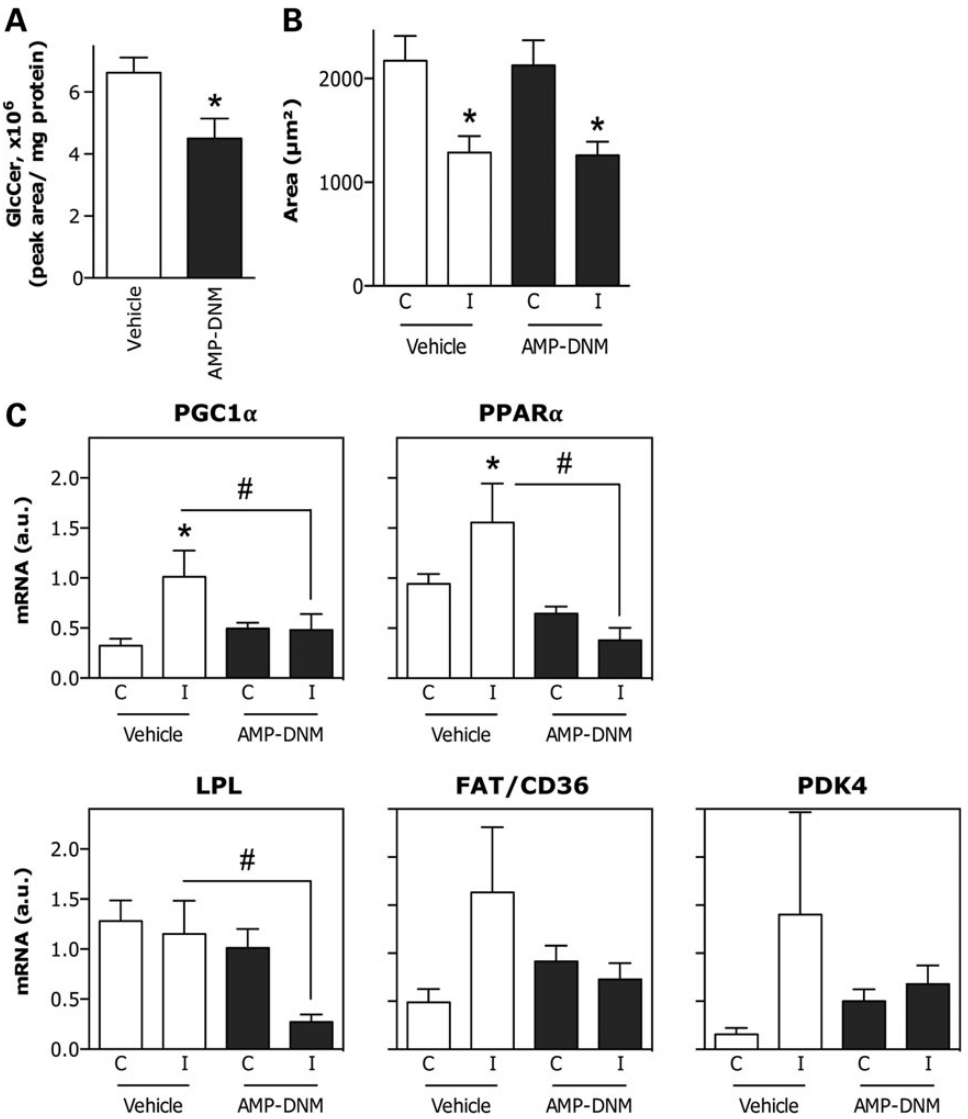

Figure 6. Effect of inhibition of GCS enzymatic activity on denervated muscle of WT mice. (**A**) HPLC quantification of GlcCer in muscle of WT mice treated with AMP-DNM. *$P < 0.05$, $n = 10$. (**B**) Cross-sectional area of fibers in muscle submitted to sciatic nerve crush in the absence (Vehicle) or presence of AMP-DNM. Ipsilateral and contralateral muscles were processed 10 days after lesion. *$P < 0.05$ versus corresponding contralateral muscle, $n = 5$. (**C**) Relative mRNA levels of PGC1α, PPARα, LPL, FAT/CD36 and PDK4 in muscle of mice as in B. *$P < 0.05$ versus corresponding contralateral muscle, #$P < 0.05$ versus vehicle, $n = 3$–8.

mice treated with AMP-DNM showed reduced hind limb grip strength (Fig. 8A). After treatment, the number of innervated synapses in treated and untreated mice was unchanged (Fig. 8B). In contrast, a more detailed analysis of the integrity of the postsynaptic apparatus revealed important morphological modifications (Fig. 8C). Specifically, the degree of fragmentation of the motor endplates was increased in treated SOD1(G86R) mice compared with untreated littermates (Fig. 8D). In addition, the number of gutter intersections per neuromuscular junction was decreased (Fig. 8E), which is interpreted as a loss of complexity. This morphological deterioration coincided with the presence of typical denervation markers, including increased expression of AChR-α and lowered expression of AChR-ε (Fig. 8F). As in the sciatic nerve crush paradigm, AMP-DNM abolished the stimulation of the expression of PPARα, LPL and PDK4, which are typically involved in favoring oxidative metabolism in ALS (11,12). In contrast, the expression of the glucose transporter GLUT4 appeared up-regulated (Fig. 8F), suggesting that GCS is involved in pathways of energy metabolism.

Discussion

This report defines important rearrangements in the lipidome of spinal cord and muscle from the mutant SOD1 mouse model of ALS, which occur well before overt neuropathology. *In silico* functional analysis of these lipidomic signatures revealed significant changes in several sphingolipids, including ceramides and GlcCer. As far as spinal cord is concerned, these findings extend those of two previous studies showing increased levels of several sphingolipids and derived GSLs in mutant SOD1 mice, as well as in patients (18,46). A major limitation of using mass spectrometric methods for assigning structures to monohexosyl ceramides in spinal cord is that it is not possible to distinguish GlcCer from galactosylceramides, as they have the same mass. It is

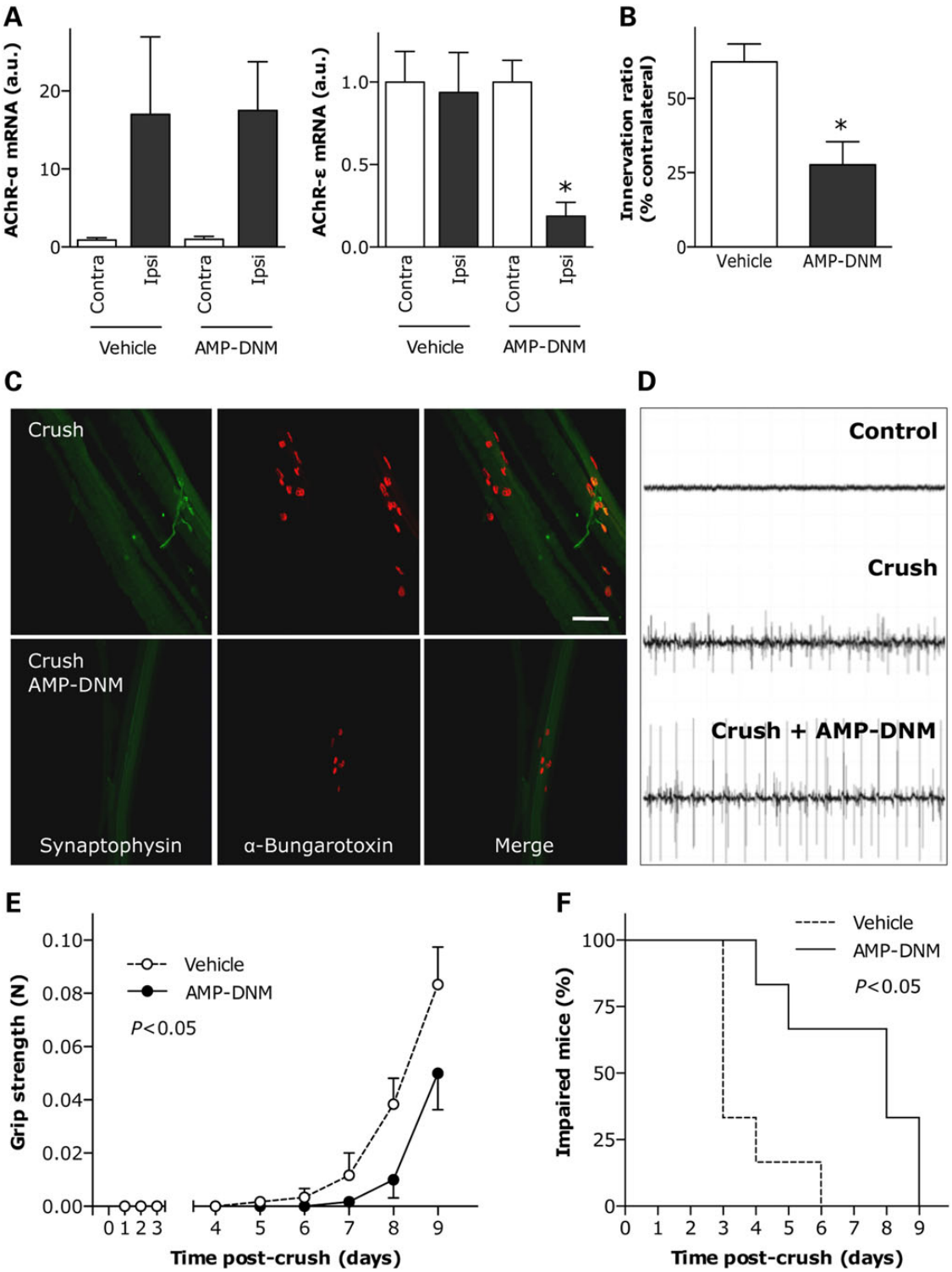

Figure 7. Effect of inhibition of GCS enzymatic activity on motor function recovery after nerve lesion in WT mice. (**A**) Relative mRNA levels of AChR-α (left panel) and AChR-ε (right panel) in muscle of WT mice submitted to sciatic nerve crush in the absence (Vehicle) or presence of AMP-DNM. Ipsilateral and contralateral muscles were processed 10 days after lesion. *$P < 0.05$ versus corresponding contralateral muscle, $n = 4$. (**B** and **C**) Proportion of properly innervated neuromuscular junctions after 10 days of sciatic nerve crush, as determined by co-labeling with anti-synaptophysin antibody (green) and rhodamine-conjugated α-bungarotoxin (red). A total of 100–150 neuromuscular junctions per animal were analyzed. Examples of labeled neuromuscular junctions are shown in C. Scale bar, 500 µm. *$P < 0.05$ versus vehicle, $n = 5$–6. (**D**) Representative electromyographic recordings in muscle of WT mice submitted to sciatic nerve crush in the absence (Crush, middle panel) or presence (Crush+AMP-DNM, lower panel) of GCS inhibitor. Upper panel shows non-denervated muscle. (**E**) Restoration of hind limb muscle grip strength in vehicle- or AMP-DNM-treated WT mice at the indicated times following sciatic nerve crush. *$P < 0.05$, $n = 5$–6. (**F**) Kaplan–Meier curves showing the proportion of WT mice unable to exhibit toe spreading as a function of time following sciatic nerve crush in the absence (vehicle) or presence of AMP-DNM. $P < 0.05$, $n = 6$.

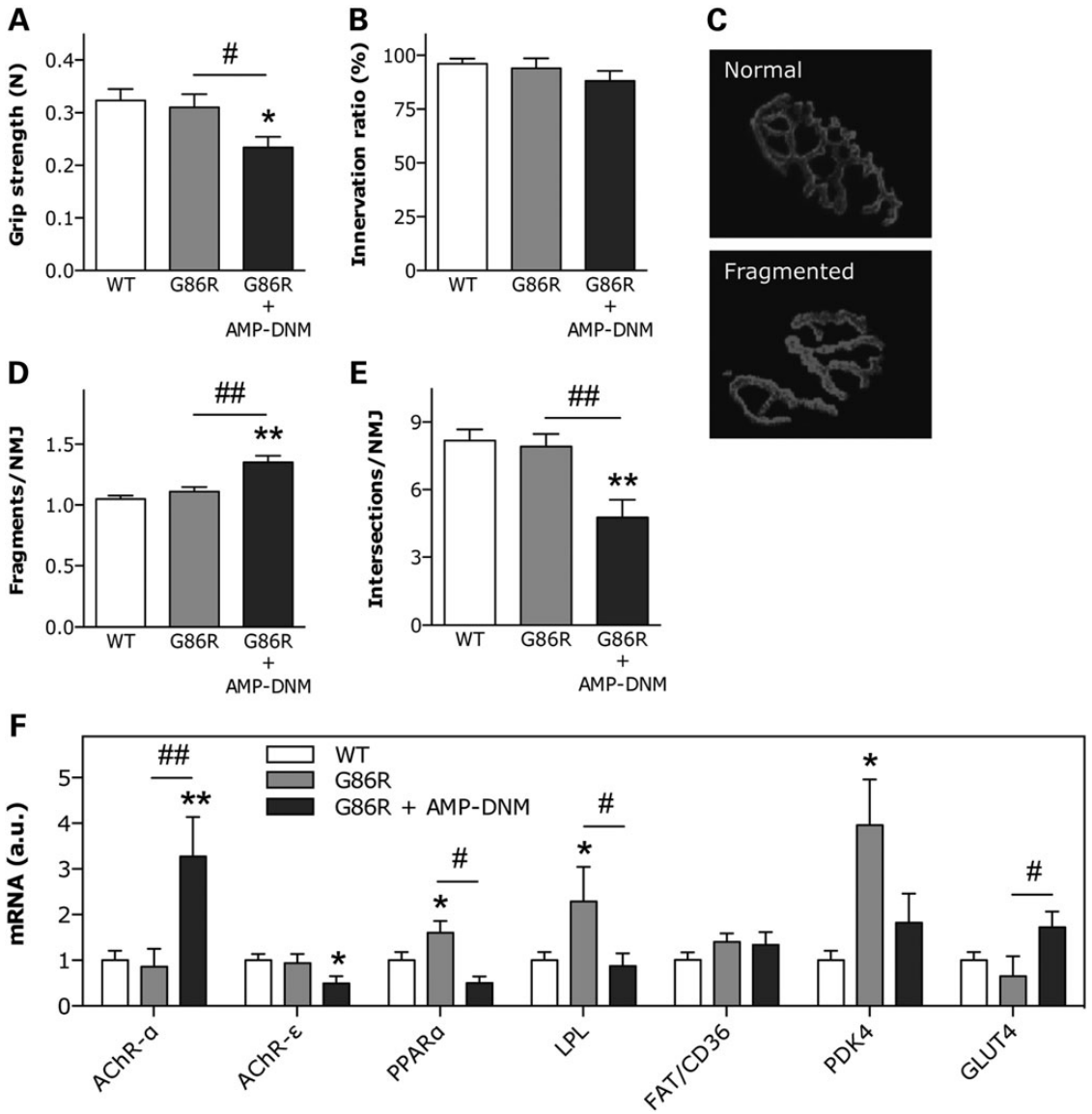

Figure 8. Effect of inhibition of GCS enzymatic activity on SOD1(G86R) mice. (**A**) Hind limb muscle grip strength in WT and SOD1(G86R) mice in the absence or presence of AMP-DNM for 10 days. $^{*}P < 0.05$ versus WT, $^{\#}P < 0.05$ versus untreated SOD1(G86R), $n = 5$–6. (**B**) Proportion of properly innervated neuromuscular junctions after 10 days of AMP-DNM treatment, as determined by co-labeling with anti-synaptophysin antibody and rhodamine-conjugated α-bungarotoxin. A total of 100–150 neuromuscular junctions per animal were counted, $n = 4$–6. Examples of normal and fragmented postsynaptic apparatus are shown in **C**. Number of separate postsynaptic gutters (**D**) and gutter intersections (**E**) per neuromuscular junction in mice as in A. A total of 20–25 neuromuscular junctions per animal were analyzed. $^{**}P < 0.01$ versus WT, $^{\#\#}P < 0.01$ versus untreated SOD1(G86R), $n = 4$. (**F**) Relative mRNA levels of AChR-α, AChR-ε, PPARα, LPL, FAT/CD36 PDK4 and GLUT4 in muscle of mice as in A. $^{*}P < 0.05$, $^{**}P < 0.01$ versus WT, $^{\#}P < 0.05$, $^{\#\#}P < 0.01$ versus untreated SOD1(G86R), $n = 4$–6.

also important to note that galactosylceramides comprise 50% of the lipid content of the central nervous system (47). Thus, we used the HPLC approach described herein to confirm the measurement of total GlcCer and GSL content in a more specific way. In spinal cord, the total amount of GlcCer, as well as the expression of GCS, was comparable between SOD1 (G86R) mice and WT littermates. In contrast, the levels of GM1a, a major ganglioside in the central nervous system, increased in spinal cord of SOD1(G86R) mice at the symptomatic stage. Interestingly, GM1 has been shown to exhibit neurotrophic properties *in vitro* (48,49) and *in vivo* (50). It is therefore tempting to suggest that the increase in GM1a we found in our mice might serve at least in part to counteract the pathological process.

A main finding of our study is that the levels of GlcCer and downstream GSLs, including GM3 and GM2, were elevated in muscle of symptomatic SOD1(G86R) mice compared with WT littermates. In addition, GCS expression in muscle was up-regulated, even during the pre-symptomatic phase of the disease. Along with this, crush injury or permanent transection of the sciatic nerve in WT mice resulted in similar muscle GCS overexpression together with significant increases in the amount of GlcCer and downstream GSLs. In all, these findings may suggest that GCS and GSLs are required in muscle in response to denervation. In support of this notion, we showed clear evidence of impeded regeneration of motor units and delayed recovery of motor function when WT mice submitted to sciatic nerve crush were treated with AMP-DNM to inhibit GCS enzymatic activity. In SOD1(G86R)

mice, AMP-DNM also triggered modifications at the physiological, histological and molecular level in muscles. The site at which GCS is essential to maintain correct neuromuscular function is unknown. Previous studies reported that neural cell-specific disruption of GCS led to demyelination of peripheral nerves (51). One can thus envisage that the detrimental effects of AMP-DNM may be the consequence of an action at the axon level.

Alternatively, specific events could also play a role. As disease progresses in mutant SOD1 mice, fast fatigable muscles convert into fatigue resistant ones, exhibiting a pronounced oxidative capacity (43). Our own previous studies revealed a switch from glucose to lipid metabolism occurring very early in the disease process (12). We also show that GCS immunostaining was present in small muscle fibers exhibiting higher oxidative capacity. These findings strongly suggest that GCS is more highly expressed in myofibers, which are typically part of the motor units most resistant to fatigue, presumably slow-twitch motor units. Potentially linking the changes in metabolism in ALS with metabolic changes following denervation, we found that the GCS inhibitor, AMP-DNM, abrogated the stimulation of the expression of several master genes involved in oxidative metabolism as part of the response of muscle to denervation and reinnervation (41,42). This phenomenon was also observed when we administered AMP-DNM to SOD1(G86R) mice, which show enhanced oxidative metabolism as part of their muscle disease phenotype (12,43). There are indeed substantial precedents for involving sphingolipids, and GSLs, in the regulation of metabolism. Induction of obesity and insulin resistance in rodents leads to an accumulation of ceramides in muscle (52,53), whereas GM3 decreases insulin signaling by forming complexes with the insulin receptor in membrane lipid rafts (54). In contrast, pharmacological inhibition of GCS reduces fatty acid accumulation and enhances insulin sensitivity in liver (44,55). In light of our present results, GCS inhibition could also influence functional recovery by acting on adaptive metabolic pathways of muscle fibers.

From a mechanistic point of view, the precise role for sphingolipids and GCS in ALS pathology needs further investigation. Hyperactive autophagy has been shown to occur in the cell bodies of motor neurons from mutant SOD1 mice, associated with the mammalian target of rapamycin complex 1 (MTORC1) pathway (56). Essentially, this pathway can be stimulated by elevated ceramide levels, which have been demonstrated both by our work and by others (18,46). An excess of ceramides thus induces autophagy and cell death, by triggering severe bioenergetic stress secondary to nutrient transporter down-regulation, whereas preservation of nutrient support inhibits this death-promoting effect (57,58). The triglyceride depletion we observed in the lipidome of muscle (and plasma) from symptomatic SOD1(G86R) mice compared with WT littermates could be interpreted as an attempt to palliate ceramide-induced autophagy and energetic stress. In line with this hypothesis, we had previously shown that feeding mutant SOD1 mice with a high fat diet re-stabilizes their energetic needs, offers neuroprotection and extends survival (10).

While this study was in final preparation, Dodge and coworkers (46) reported a similar dysfunction in GSL metabolism in animals and man, which is complementary to our data. Dodge and coworkers analyzed the effects on spinal cord whereas we examined spinal cord and muscle. Thus, both studies independently confirm a novel biochemical pathway in ALS, which has been shown to have therapeutic applications in other disorders. Both studies reveal that GCS inhibitors may be deleterious. Dodge and coworkers showed a shortening of survival in mutant SOD1 mice when the inhibitor was applied directly to the central nervous system. Here, we show that another inhibitor, administered peripherally, lowers the level of GlcCer, blocks the expression program of metabolic genes in response to denervation, as well as delays regeneration of motor units and recovery of motor function in mice submitted to nerve injury. We also show that GCS is dysregulated in muscle of ALS patients and may aggregate with TDP-43, a phenomenon that could have pathological relevance for the more frequent sporadic forms of the disease. In this context, manipulating GCS and GlcCer metabolism pharmacologically could pave the way for developing novel therapeutic strategies to palliate motor neuron injury. Our present findings provide compelling evidence for the importance of lipid metabolism in ALS, as well as a novel role for GCS in ALS muscle pathology.

Materials and Methods

Animals

FVB/N male mice, overexpressing SOD1(G86R), were maintained in our animal facility at 23°C with a 12 h light/dark cycle. Genotyping was performed according to Ripps and coworkers (5). Mice had water and regular A04 rodent chow *ad libitum* and were fasted overnight before sacrifice. At 75 days of age (referred as to the pre-symptomatic group), mice were without signs of motor impairment, as determined by the absence of electromyographic abnormalities, as well as muscle expression of AChR-α and number of spinal cord motor neurons comparable to WT mice. At ~100 days of age (referred as to the symptomatic group), mice showed apparent signs of paresis, or partial paralysis, in at least one limb, coinciding with the alteration of the above-mentioned parameters (59). WT male littermates served as controls. To induce peripheral nerve injury, mice were anesthetized with ketamine chlorohydrate (100 mg/kg) and xylazine (5 mg/kg). The sciatic nerve was exposed at mid-thigh level and crushed with fine forceps for 30 s, or a 3-mm section removed with microscissors. The skin incision was sutured, and mice were allowed to recover. The hind limb, contralateral to the lesion, served as control. To inhibit GCS enzymatic activity, mice subjected to sciatic nerve crush were treated with daily intraperitoneal injections of N-(5-adamantane-1-yl-methoxy-pentyl)-deoxynojirimycin (AMP-DNM, Cayman Chemical Company, Ann Arbor, MI) for 10 days, the typical time frame required for recovery of motor function under normal conditions. AMP-DNM was prepared and given as a daily dose of 25 mg/kg in 0.9% NaCl containing 5% DMSO (44). Mice were killed by decapitation after deep anesthesia with 120 mg/kg sodium pentobarbital. Lumbar spinal cord and muscle were rapidly dissected, frozen in liquid nitrogen and stored at −80°C. For immunolabeling experiments, dissected muscle samples were fixed with 4% paraformaldehyde and stored in PBS at 4°C. Experiments followed current European Union regulations (Directive 2010/63/EU) and were performed by authorized investigators (license from *Prefecture du Bas-Rhin* No. A67-402 to A.H.), after approval by the ethics committee of the University of Strasbourg (license No. AL/01/20/09/12, AL/02/21/09/12 and AL/15/44/12/12).

Patients

A retrospective case–control study was performed with 14 ALS patients and 16 control subjects recruited from 2 referral centers for ALS located in Strasbourg (France) and Ulm (Germany). Patients diagnosed as having probable or definite ALS, according to the revised El Escorial criteria (60), were included. Control subjects were diagnosed as having fibromyalgia and were enrolled as

part of the routine diagnostic examination protocol. Muscle biopsies from four control subjects and six ALS patients (recruited in Ulm) were processed for immunohistochemistry studies. Muscle biopsies from other 12 control subjects and 8 ALS patients (recruited in Strasbourg) were used for gene expression studies. All individuals gave informed consent, and the study was approved by the institutional ethical committees of the University Hospital of Strasbourg (CPP 09/40, No AC 2008-438, No. DC 2009-1002) and the University of Ulm (Authorization No. 12/09).

Lipid extraction

Tissue samples (25 mg for lumbar spinal cord, and 25–50 mg for soleus muscle) were gently thawed on crushed ice and homogenized with 335 µl precooled methanol. Lipids were extracted by orbital agitation using a Precellys system (Bertin Technologies, Saint-Quentin-en-Yvelines, France) in a propylene tube containing ceramic beads. Two homogenization steps at 5000 rpm for 30 s each were performed at room temperature. Homogenates were transferred into glass conic tubes. To recover the maximum volume of homogenate, Precellys tubes, beads and tips were washed with additional 335 µl precooled methanol. Then, homogenates were mixed with 1340 µl chloroform and centrifuged at 2000 rpm for 5 min at 4°C. The organic phase was transferred into a conical glass tube and washed with 400 µl precooled 0.9% NaCl. After centrifugation at 2000 rpm for 5 min at 4°C, the organic phase was evaporated to dryness at 30°C under nitrogen. Residues were reconstituted with acetonitrile/isopropanol (1:1) (100 µl for lumbar spinal cord, and 60 µl for soleus muscle) and further diluted with solvent mixture before injection (1/40 for lumbar spinal cord, and 1/10 for soleus muscle).

UPLC/TOF-MS

Chromatography was performed on an Acquity UPLC system using an Acquity BEH C18 column (100 mm × 2.1 mm, 1.7 µm, Waters Corporation, Milford, MA) maintained at 50°C. Chromatographic flow rate was 0.5 ml/min, and run time was 18 min. Mobile phases were isopropanol (solvent A) and acetonitrile (solvent B). The starting condition was 100% solvent B, followed by a gradual increase (gradient type 6) of solvent A from 0 to 75% over the first 15 min. Then, 100% solvent B was reused from 15.1 to 17 min. The chromatographic system was coupled to a Micromass LCT Premier TOF/W mass spectrometer (Waters Corporation), equipped with an electrospray source operating in positive ion mode with a lockspray interface for accurate mass measurements. Source temperature was set at 150°C, with a cone gas flow of 50 l/h at 400°C and a nebulization gas flow of 750 l/h. Capillary voltage was set at 2.7 kV, with a cone voltage of 50 V. Scan acquisition time was 0.1 s, and interscan delay was 0.01 s, in dynamic range enhancement mode. Leucine enkephalin was used as lockmass compound, infused at a concentration of 50 pg/µl at an infusion flow rate of 50 µl/min. Isotopic [M+H]+ ions of leucine enkephalin at 558.2829 and 556.2771 were used for normal and attenuated lock mass mode, respectively. Mass spectral data were acquired in centroid mode over the mass range m/z 200–1200. Samples were injected in a specific run order, following an orthogonal way according to study design, to take into account the signal drift of the mass spectrometer over the run time (61).

HPLC

GlcCer and downstream GSLs were analyzed essentially as described by Neville and coworkers (62). Lumbar spinal cord and soleus muscle were homogenized in water using an Ultraturax T25 probe homogenizer (IKA, Germany). Lipids from tissue homogenates were extracted with chloroform and methanol. The GSLs were then further purified using solid-phase C18 columns (Telos, Kinesis, UK). After elution, the GSL fractions were split in half, dried down under nitrogen at 42°C and treated with either Cerezyme® (Genzyme, Cambridge, MA) to obtain glucose from GlcCer or ceramide glycanase (prepared *in house* from the medicinal leech *Hirudo medicinalis/verbena*) to obtain oligosaccharides from other GSLs. The liberated glucose and free glycans were then fluorescently-labeled with anthranillic acid (2-AA). To remove excess free label, samples were separated in 6S SPE columns (Supelco, PA, USA). Purified 2AA-labeled glucose and 2AA-labeled oligosaccharides were separated and qualified by normal-phase high-performance liquid chromatography (NP-HPLC) as previously described (62). The solid phase used was a 4.6 × 250 mm TSK gel-Amide 80 column (Anachem, Luton, UK). The HPLC system consisted of a Waters Alliance 2695 separations module and an in-line Waters 2475 multi λ_fluorescence detector set at Ex λ_360 nm and Em λ_425 nm.

Quantitative RT–PCR

Total RNA was prepared by standard protocol. Briefly, frozen samples of lumbar spinal cord, and gastrocnemius or tibialis anterior muscle were placed on ice into a tube containing a 5-mm stainless steel bead. 1 ml Trizol reagent (Invitrogen, Groningen, The Netherlands) was added, and homogenization was performed in a TissueLyser (Qiagen, Valencia, CA) at 30 Hz for 3 min twice. RNA was extracted with chloroform/isopropyl alcohol/ethanol and stored at −80°C until use. One microgram of total RNA was used to synthesize cDNA using Iscript reverse transcriptase (BioRad, Marnes La Coquette, France) and oligo-dT primer as specified by the manufacturer. Gene expression was measured on a Bio-Rad iCycler using SYBR green reagent (2× SYBR Green Supermix, BioRad) according to manufacturer's instructions. PCR was performed in optimized conditions: denaturation at 95°C for 3 min, followed by 40 cycles of 10 s at 95°C and 30 s at 60°C. Primers from Eurogentec (Seraing, Belgium) are shown in Supplementary Material, Table S4. Relative quantification was achieved by calculating the ratio between the cycle number (Ct) at which the signal crossed a threshold set within the logarithmic phase of the gene of interest and that of the 18S reference gene. Ct values were the means of duplicates.

Western blot

Tibialis anterior muscle samples were rapidly dissected on ice and homogenized with TissueLyser (Qiagen) three times at 30 Hz for 3 min each, in PBS containing 1% protease inhibitor cocktail. Homogenates were digested with 0.2 mg/ml collagenase (Sigma–Aldrich, Lyon, France) by gentle agitation for 30 min at room temperature. Then, samples were incubated for 1 h at room temperature with gentle agitation in 2 volumes of Ripa buffer (50 mm Tris–HCl pH 8, 150 mm NaCl, 1% Triton X-100, 0.1% SDS, 0.5% sodium deoxycholate and 1 mm EDTA), containing 0.01% digitonin. Equal amounts of protein, according to the bicinchoninic acid assay (Uptima Interchim, Montluçon, France), were mixed with Laemmli sample buffer (0.05 m Tris–HCl pH 6.8, 2% SDS, 2% β-mercaptoethanol, 8% glycerol and bromophenol blue), boiled for 5 min and separated on a 4–20% Criterion Stain Free SDS–polyacrylamide gel (BioRad). Separated proteins were electrotransferred to nitrocellulose membranes and subjected to reversible staining with 0.1% Ponceau S in 5% acetic

acid to ensure homogeneous transfer. Immunostaining was performed with a rabbit polyclonal anti-GCS antibody (Proteintech, Manchester, UK) diluted 1/200, and horseradish peroxidase-conjugated goat anti-rabbit IgG (Abliance, Compiègne, France) diluted 1/1000. Actin was detected by using a rabbit polyclonal anti-actin antibody (Sigma–Aldrich) diluted 1/20 000. Blots were developed with SuperSignal West Pico Chemiluminescent Substrate (Thermo Fisher, Courtaboeuf, France) and visualized with ChemiDoc XRS+ (BioRad).

Immunoperoxidase staining

Mouse gastrocnemius muscle samples were frozen in isopentane, precooled with liquid nitrogen and cut with a cryostat into 20-µm-thick cross-sections. GCS immunoreactivity was detected with a rabbit polyclonal antibody diluted 1/100 (Proteintech). Antibody binding was detected using a standard indirect immunoperoxidase technique, with goat anti-rabbit IgG-biotin conjugate diluted 1/500 (Proteintech) and Vectastain ABC kit (Vector Laboratories, Burlingame, CA). Human muscle biopsies (Table 2) were processed as above, and immunostaining was performed identically, except that GCS and TDP-43 antibodies (Proteintech), both diluted 1/100, were applied to adjacent sections, respectively, to ensure that their immunoreactivities could be seen within the same myofibers. Omission of primary antisera was performed to verify the specificity of the immunoreaction. Photomicrographs were taken with a Nikon microscope, and cross-sectional areas of myofibers were measured with NIH IMAGE 1.62.

Muscle histochemistry

The standard histochemical assay for SDH was used to distinguish between oxidative and non-oxidative muscle fibers. Twenty-micrometer sections were obtained by cutting isopentane fresh-frozen muscles perpendicular to the muscle axis with a cryostat at −20°C (Leica, Nanterre, France). Sections were fixed with acetone for 15 min, air-dried and incubated for 30 min at 37°C in a solution containing 10 g/l sodium succinate, 2 g/l nitro blue tetrazolium and 0.025 g/l phenazine methosulfate. After washing, sections were mounted with aqueous mounting medium (Dako, Trappes, France). Photomicrographs were obtained with a Nikon microscope at a magnification of ×200 on sections adjacent to those used for GCS immunostaining.

Toe reflex spreading test

Toe spread was manually monitored for each hind limb as an index of motor recovery after sciatic nerve lesion (45). Mice were scruffed, held supine and spacing between toes was measured. Onset of toe spreading was defined by a distance of at least one millimeter between two consecutive toes on the ipsilateral side of the lesion.

Muscle grip strength

Muscle strength was determined using the grip test (Bioseb, Chaville, France). Mice were placed over a metallic grid that they instinctively grab to try to stop the involuntary backward movement carried out by the manipulator until the pulling force overcomes their grip strength. After the animal loses its grip, the strength-meter scores the peak pull force. Strength was measured independently in hind limbs ipsi- and contralateral to the nerve lesion, and the mean of three assays was scored for each animal.

Electromyography

Recordings were obtained with a standard electromyography apparatus (Dantec, Les Ulis, France), in accordance with the guidelines of the American Association of Electrodiagnostic Medicine. Mice were anesthetized as indicated above and kept under a heating lamp to maintain physiological muscle temperature. A concentric needle electrode (no. 9013S0011, diameter 0.3 mm; Medtronic, Minneapolis, MN) was inserted in the gastrocnemius, and a monopolar needle electrode (no. 9013R0312, diameter 0.3 mm; Medtronic) was inserted into the tail of the animal to ground the system. Each muscle was monitored in three different regions, and the degree of denervation was scored as the number of regions with spontaneous activity expressed as a percentage. Only spontaneous activity with peak-to-peak amplitude of at least 50 µV was considered to be significant.

Neuromuscular junction labeling

Tibialis anterior muscle samples were dissected into thin bundles under a binocular microscope. Bundles were collected from at least three different parts of the muscle. Acetylcholine receptors in the postsynaptic apparatus of neuromuscular junctions were labeled with rhodamine-conjugated α-bungarotoxin (Sigma–Aldrich). Immunofluorescent labeling of nerve terminals was performed with a rabbit polyclonal anti-synaptophysin antibody diluted 1/200 (Abcam, Cambridge, UK), and Alexa-conjugated goat anti-rabbit IgG diluted 1/500 (Jackson ImmunoResearch, Suffolk, UK). Muscle bundles were mounted onto slides, prior to fluorescence microscopy. Neuromuscular junctions were considered as denervated when the presynaptic nerve terminal was absent from the postsynaptic region. Integrity of the typical pretzel-shaped morphology of neuromuscular junctions was determined as previously described (63) by quantifying the number of separate postsynaptic gutters, which estimates the degree of fragmentation, and the number of gutter intersections, which estimates the degree of enlargement and complexity of the postsynaptic apparatus.

Statistical analysis

For lipidomics data, chromatogram alignment, blank and chemical noise subtraction and subsequent peak selection were achieved with Refiner MS 6.0 (Genedata, Basel, Switzerland), to obtain a list of molecular features common to each set of mice (61). Data with retention times between 0.5 and 15 min and peak intensity distinct from zero were retained, normalized to fresh tissue mass and mean-centered with reference to the presymptomatic group. Data were submitted to PARETO transformation before statistical analysis. To define differences between SOD1(G86R) mice and WT littermates, score plots were generated by unsupervised multivariate PCA, using SIMCA-P 12.0 (Umetrics, Umea, Sweden). Specific changes between experimental groups were further identified by using supervised multivariate orthogonal partial least-squares discriminant analysis (PLS-DA), as implemented in SIMCA-P (61,64). For each molecular feature, a SOD1 (G86R)-to-WT ratio was calculated. This was considered significant if the corresponding variable correlation coefficient was less than or equal to −0.7 or greater than or equal to +0.7, according to the p(corr) coordinate in the S-plot built after the PLS-DA model. Molecular features with significant changes were associated with theoretically identified metabolites based on their atomic mass (m/z), by using online HMDB 2.5 and METLIN databases (29,30). Over-represented pathways were identified with ConsensusPathDB (31), and joint enrichment analysis of

transcriptomics and lipidomics data was performed using IMPaLA (33). The flowchart for data mining is shown in Supplementary Material, Figure S1. Non-lipidomics data, unless otherwise indicated, were expressed as the mean ± SEM and were analyzed with PRISM 6.0b (GraphPad, San Diego, CA). Student's t test was used to compare two groups, and ANOVA followed by Fisher's LSD test was applied to compare more than two groups. Grip strength curves were analyzed with two-way ANOVA, and survival curves were analyzed with Log-rank test. Differences with *P*-values of <0.05 were considered significant.

Supplementary Material

Supplementary Material is available at *HMG* online.

Acknowledgements

We thank Annie Picchinenna, Marie José Ruivo and Claire Weber for excellent technical assistance. We also acknowledge the patients and their families.

Conflict of Interest statement: The funders had no role in study design, data collection and analysis, decision to publish or preparation of the manuscript.

Funding

This work was supported by 'Appel à Projets 2009 du Conseil Scientifique' (University of Strasbourg), European Community's Health Seventh Framework Programme under grant agreement No. 259867 (Euro-MOTOR), 'Les Laboratoires Servier', Target ALS and 'Association André combat la SLA'. A.H. is a research fellow receiving funds from Euro-MOTOR. G.H. was supported by the Higher Education Commission of the Pakistani government and 'Association pour la Recherche et le Développement de Moyens de Lutte contre les Maladies Neurodégénératives' (AREMANE). J.L.G.D.A. was recipient of a 'Chaire d'Excellence INSERM/Université de Strasbourg'. Funding to pay the Open Access publication charges for this article was provided by Target ALS.

References

1. Kiernan, M.C., Vucic, S., Cheah, B.C., Turner, M.R., Eisen, A., Hardiman, O., Burrell, J.R. and Zoing, M.C. (2011) Amyotrophic lateral sclerosis. *Lancet*, **377**, 942–955.
2. Rosen, D.R., Siddique, T., Patterson, D., Figlewicz, D.A., Sapp, P., Hentati, A., Donaldson, D., Goto, J., O'Regan, J.P., Deng, H. X. *et al*. (1993) Mutations in Cu/Zn superoxide dismutase gene are associated with familial amyotrophic lateral sclerosis. *Nature*, **362**, 59–62.
3. Renton, A.E., Chiò, A. and Traynor, B.J. (2014) State of play in amyotrophic lateral sclerosis genetics. *Nat. Neurosci.*, **17**, 17–23.
4. Gurney, M.E., Pu, H., Chiu, A.Y., Dal Canto, M.C., Polchow, C.Y., Alexander, D.D., Caliendo, J., Hentati, A., Kwon, Y.W., Deng, H. X. *et al*. (1994) Motor neuron degeneration in mice that express a human Cu, Zn superoxide dismutase mutation. *Science*, **264**, 1772–5.
5. Ripps, M.E., Huntley, G.W., Hof, P.R., Morrison, J.H. and Gordon, J.W. (1995) Transgenic mice expressing an altered murine superoxide dismutase gene provide an animal model of amyotrophic lateral sclerosis. *Proc. Natl Acad. Sci. USA*, **92**, 689–693.
6. Wong, P.C., Pardo, C.A., Borchelt, D.R., Lee, M.K., Copeland, N. G., Jenkins, N.A., Sisodia, S.S., Cleveland, D.W. and Price, D.L. (1995) An adverse property of a familial ALS-linked SOD1 mutation causes motor neuron disease characterized by vacuolar degeneration of mitochondria. *Neuron*, **14**, 1105–1116.
7. Desport, J.C., Torny, F., Lacoste, M., Preux, P.M. and Couratier, P. (2005) Hypermetabolism in ALS: correlations with clinical and paraclinical parameters. *Neurodegener. Dis.*, **2**, 202–207.
8. Dupuis, L., Pradat, P.F., Ludolph, A.C. and Loeffler, J.P. (2011) Energy metabolism in amyotrophic lateral sclerosis. *Lancet Neurol.*, **10**, 75–82.
9. Schmitt, F., Hussain, G., Dupuis, L., Loeffler, J.P. and Henriques, A. (2014) A plural role for lipids in motor neuron diseases: energy, signaling and structure. *Front. Cell. Neurosci.*, **8**, 25.
10. Dupuis, L., Oudart, H., René, F., Gonzalez De Aguilar, J.L. and Loeffler, J.P. (2004) Evidence for defective energy homeostasis in amyotrophic lateral sclerosis: benefit of a high-energy diet in a transgenic mouse model. *Proc. Natl Acad. Sci. USA*, **101**, 11159–11164.
11. Fergani, A., Oudart, H., Gonzalez De Aguilar, J.L., Fricker, B., René, F., Hocquette, J.F., Meininger, V., Dupuis, L. and Loeffler, J.P. (2007) Increased peripheral lipid clearance in an animal model of amyotrophic lateral sclerosis. *J. Lipid Res.*, **48**, 1571–1580.
12. Palamiuc, L., Schlagowski, A., Ngo, S.T., Vernay, A., Dirrig-Grosch, S., Henriques, A., Boutillier, A.L., Zoll, J., Echaniz-Laguna, A., Loeffler, J.P. and René, F. (2015) A metabolic switch toward lipid use in glycolytic muscle is an early pathologic event in a mouse model of amyotrophic lateral sclerosis. *EMBO Mol. Med.*, **7**, 526–546.
13. Dupuis, L., Corcia, P., Fergani, A., Gonzalez De Aguilar, J.L., Bonnefont-Rousselot, D., Bittar, R., Seilhean, D., Hauw, J.J., Lacomblez, L., Loeffler, J.P. and Meininger, V. (2008) Dyslipidemia is a protective factor in amyotrophic lateral sclerosis. *Neurology*, **70**, 1004–1009.
14. Dorst, J., Kühnlein, P., Hendrich, C., Kassubek, J., Sperfeld, A. D. and Ludolph, A.C. (2011) Patients with elevated triglyceride and cholesterol serum levels have a prolonged survival in amyotrophic lateral sclerosis. *J. Neurol.*, **258**, 613–617.
15. Paganoni, S., Deng, J., Jaffa, M., Cudkowicz, M.E. and Wills, A. M. (2011) Body mass index, not dyslipidemia, is an independent predictor of survival in amyotrophic lateral sclerosis. *Muscle Nerve*, **44**, 20–24.
16. Sutedja, N.A., van der Schouw, Y.T., Fischer, K., Sizoo, E.M., Huisman, M.H., Veldink, J.H. and Van den Berg, L.H. (2011) Beneficial vascular risk profile is associated with amyotrophic lateral sclerosis. *J. Neurol. Neurosurg. Psychiatry*, **82**, 638–642.
17. Henriques, A., Blasco, H., Fleury, M.C., Corcia, P., Echaniz-Laguna, A., Robelin, L., Rudolf, G., Lequeu, T., Bergaentzle, M., Gachet, C. *et al*. (2015) Blood cell palmitoleate-palmitate ratio is an independent prognostic factor for amyotrophic lateral sclerosis. *PLoS One*, **10**, e0131512.
18. Cutler, R.G., Pedersen, W.A., Camandola, S., Rothstein, J.D. and Mattson, M.P. (2002) Evidence that accumulation of ceramides and cholesterol esters mediates oxidative stress-induced death of motor neurons in amyotrophic lateral sclerosis. *Ann. Neurol.*, **52**, 448–457.
19. Ilieva, E.V., Ayala, V., Jové, M., Dalfó, E., Cacabelos, D., Povedano, M., Bellmunt, M.J., Ferrer, I., Pamplona, R. and Portero-Otín, M. (2007) Oxidative and endoplasmic reticulum stress interplay in sporadic amyotrophic lateral sclerosis. *Brain*, **130**(Pt 12), 3111–3123.
20. Rozen, S., Cudkowicz, M.E., Bogdanov, M., Matson, W.R., Kristal, B.S., Beecher, C., Harrison, S., Vouros, P., Flarakos, J., Vigneau-Callahan, K. *et al*. (2005) Metabolomic analysis and signatures in motor neuron disease. *Metabolomics*, **1**, 101–108.

21. Blasco, H., Corcia, P., Moreau, C., Veau, S., Fournier, C., Vourc'h, P., Emond, P., Gordon, P., Pradat, P.F., Praline, J. *et al.* (2010) 1H-NMR-based metabolomic profiling of CSF in early amyotrophic lateral sclerosis. *PLoS ONE*, **5**, e13223.
22. Kumar, A., Bala, L., Kalita, J., Misra, U.K., Singh, R.L., Khetrapal, C.L. and Babu, G.N. (2010) Metabolomic analysis of serum by (1) H NMR spectroscopy in amyotrophic lateral sclerosis. *Clin. Chim. Acta*, **411**, 563–567.
23. Wuolikainen, A., Moritz, T., Marklund, S.L., Antti, H. and Andersen, P.M. (2011) Disease-related changes in the cerebrospinal fluid metabolome in amyotrophic lateral sclerosis detected by GC/TOFMS. *PLoS ONE*, **6**, e17947.
24. Lawton, K.A., Cudkowicz, M.E., Brown, M.V., Alexander, D., Caffrey, R., Wulff, J.E., Bowser, R., Lawson, R., Jaffa, M., Milburn, M.V. *et al.* (2012) Biochemical alterations associated with ALS. *Amyotroph. Lateral Scler.*, **13**, 110–118.
25. Wuolikainen, A., Andersen, P.M., Moritz, T., Marklund, S.L. and Antti, H. (2012) ALS patients with mutations in the SOD1 gene have an unique metabolomic profile in the cerebrospinal fluid compared with ALS patients without mutations. *Mol. Genet. Metab.*, **105**, 472–478.
26. Blasco, H., Corcia, P., Pradat, P.F., Bocca, C., Gordon, P.H., Veyrat-Durebex, C., Mavel, S., Nadal-Desbarats, L., Moreau, C., Devos, D. *et al.* (2013) Metabolomics in cerebrospinal fluid of patients with amyotrophic lateral sclerosis: an untargeted approach via high-resolution mass spectrometry. *J. Proteome Res.*, **12**, 3746–3754.
27. Chan, E.C., Yap, S.L., Lau, A.J., Leow, P.C., Toh, D.F. and Koh, H. L. (2007) Ultra-performance liquid chromatography/time-of-flight mass spectrometry based metabolomics of raw and steamed Panax notoginseng. *Rapid Commun. Mass Spectrom.*, **21**, 519–528.
28. Ishibashi, Y., Kohyama-Koganeya, A. and Hirabayashi, Y. (2013) New insights on glucosylated lipids: metabolism and functions. *Biochim. Biophys. Acta*, **1831**, 1475–1485.
29. Wishart, D.S., Knox, C., Guo, A.C., Eisner, R., Young, N., Gautam, B., Hau, D.D., Psychogios, N., Dong, E., Bouatra, S. *et al.* (2009) HMDB: a knowledgebase for the human metabolome. *Nucl. Acids Res.*, **37**, D603–D610.
30. Tautenhahn, R., Cho, K., Uritboonthai, W., Zhu, Z., Patti, G. and Siuzdak, G. (2012) An accelerated workflow for untargeted metabolomics using the METLIN database. *Nature Biotechnol.*, **30**, 826–828.
31. Kamburov, A., Pentchev, K., Galicka, H., Wierling, C., Lehrach, H. and Herwig, R. (2011) ConsensusPathDB: toward a more complete picture of cell biology. *Nucl. Acids Res.*, **39**, D712–D717.
32. Gonzalez De Aguilar, J.L., Niederhauser-Wiederkehr, C., Halter, B., De Tapia, M., Di Scala, F., Demougin, P., Dupuis, L., Primig, M., Meininger, V. and Loeffler, J.P. (2008) Gene profiling of skeletal muscle in an amyotrophic lateral sclerosis mouse model. *Physiol. Genomics*, **32**, 207–218.
33. Kamburov, A., Cavill, R., Ebbels, T.M., Herwig, R. and Keun, H. C. (2011) Integrated pathway-level analysis of transcriptomics and metabolomics data with IMPaLA. *Bioinformatics*, **27**, 2917–2918.
34. Bruni, P. and Donati, C. (2008) Pleiotropic effects of sphingolipids in skeletal muscle. *Cell. Mol. Life Sci.*, **65**, 3725–3736.
35. Jennemann, R. and Gröne, H.J. (2013) Cell-specific in vivo functions of glycosphingolipids: lessons from genetic deletions of enzymes involved in glycosphingolipid synthesis. *Prog. Lipid Res.*, **52**, 231–248.
36. Jasmin, B.J., Cartaud, J., Bornens, M. and Changeux, J.P. (1989) Golgi apparatus in chick skeletal muscle: changes in its distribution during end plate development and after denervation. *Proc. Natl Acad. Sci. USA*, **86**, 7218–7222.
37. Neumann, M., Sampathu, D.M., Kwong, L.K., Truax, A.C., Micsenyi, M.C., Chou, T.T., Bruce, J., Schuck, T., Grossman, M., Clark, C.M. *et al.* (2006) Ubiquitinated TDP-43 in frontotemporal lobar degeneration and amyotrophic lateral sclerosis. *Science*, **314**, 130–133.
38. Weihl, C.C., Temiz, P., Miller, S.E., Watts, G., Smith, C., Forman, M., Hanson, P.I., Kimonis, V. and Pestronk, A. (2008) TDP-43 accumulation in inclusion body myopathy muscle suggests a common pathogenic mechanism with frontotemporal dementia. *J. Neurol. Neurosurg. Psychiatry*, **79**, 1186–1189.
39. Cortese, A., Plagnol, V., Brady, S., Simone, R., Lashley, T., Acevedo-Arozena, A., de Silva, R., Greensmith, L., Holton, J., Hanna, M.G. *et al.* (2014) Widespread RNA metabolism impairment in sporadic inclusion body myositis TDP43-proteinopathy. *Neurobiol. Aging*, **35**, 1491–1498.
40. Kilbey, A., Terry, A., Jenkins, A., Borland, G., Zhang, Q., Wakelam, M.J., Cameron, E.R. and Neil, J.C. (2010) Runx regulation of sphingolipid metabolism and survival signaling. *Cancer Res.*, **70**, 5860–5869.
41. Lowrie, M.B., Krishnan, S. and Vrbová, G. (1982) Recovery of slow and fast muscles following nerve injury during early post-natal development in the rat. *J. Physiol.*, **331**, 51–66.
42. Navarrete, R. and Vrbová, G. (1984) Differential effect of nerve injury at birth on the activity pattern of reinnervated slow and fast muscles of the rat. *J. Physiol.*, **351**, 675–685.
43. Sharp, P.S., Dick, J.R. and Greensmith, L. (2005) The effect of peripheral nerve injury on disease progression in the SOD1 (G93A) mouse model of amyotrophic lateral sclerosis. *Neuroscience*, **130**, 897–910.
44. Aerts, J.M., Ottenhoff, R., Powlson, A.S., Grefhorst, A., van Eijk, M., Dubbelhuis, P.F., Aten, J., Kuipers, F., Serlie, M.J., Wennekes, T. *et al.* (2007) Pharmacological inhibition of glucosylceramide synthase enhances insulin sensitivity. *Diabetes*, **56**, 1341–1349.
45. Deumens, R., Jaken, R.J., Marcus, M.A. and Joosten, E.A. (2007) The CatWalk gait analysis in assessment of both dynamic and static gait changes after adult rat sciatic nerve resection. *J. Neurosci. Methods*, **164**, 120–130.
46. Dodge, J.C., Treleaven, C.M., Pacheco, J., Cooper, S., Bao, C., Abraham, M., Cromwell, M., Sardi, S.P., Chuang, W.L., Sidman, R.L. *et al.* (2015) Glycosphingolipids are modulators of disease pathogenesis in amyotrophic lateral sclerosis. *Proc. Natl Acad. Sci. USA*, **112**, 8100–8105.
47. Cuzner, M.L., Davison, A.N. and Gregson, N.A. (1965) The chemical composition of vertebrate myelin and microsomes. *J. Neurochem.*, **12**, 469–481.
48. Huang, F., Dong, X., Zhang, L., Zhang, X., Zhao, D., Bai, X. and Li, Z. (2009) The neuroprotective effects of NGF combined with GM1 on injured spinal cord neurons in vitro. *Brain Res. Bull.*, **79**, 85–88.
49. Huang, F., Dong, X., Zhang, L., Zhang, X., Zhao, D., Bai, X. and Li, Z. (2010) GM1 and nerve growth factor modulate mitochondrial membrane potential and neurofilament light mRNA expression in cultured dorsal root ganglion and spinal cord neurons during excitotoxic glutamate exposure. *J. Clin. Neurosci.*, **17**, 495–500.
50. Leake, P.A., Hradek, G.T., Vollmer, M. and Rebscher, S.J. (2007) Neurotrophic effects of GM1 ganglioside and electrical stimulation on cochlear spiral ganglion neurons in cats deafened as neonates. *J. Comp. Neurol.*, **501**, 837–853.
51. Jennemann, R., Sandhoff, R., Wang, S., Kiss, E., Gretz, N., Zuliani, C., Martin-Villalba, A., Jäger, R., Schorle, H., Kenzelmann, M.

et al. (2005) Cell-specific deletion of glucosylceramide synthase in brain leads to severe neural defects after birth. *Proc. Natl Acad. Sci. USA*, **102**, 12459–12464.
52. Chavez, J.A., Siddique, M.M., Wang, S.T., Ching, J., Shayman, J.A. and Summers, S.A. (2014) Ceramides and glucosylceramides are independent antagonists of insulin signaling. *J. Biol. Chem.*, **289**, 723–734.
53. Mason, R.R., Mokhtar, R., Matzaris, M., Selathurai, A., Kowalski, G.M., Mokbel, N., Meikle, P.J., Bruce, C.R. and Watt, M.J. (2014) PLIN5 deletion remodels intracellular lipid composition and causes insulin resistance in muscle. *Mol. Metab.*, **3**, 652–663.
54. Kabayama, K., Sato, T., Saito, K., Loberto, N., Prinetti, A., Sonnino, S., Kinjo, M., Igarashi, Y. and Inokuchi, J. (2007) Dissociation of the insulin receptor and caveolin-1 complex by ganglioside GM3 in the state of insulin resistance. *Proc. Natl Acad. Sci. USA*, **104**, 13678–13683.
55. Lombardo, E., van Roomen, C.P., van Puijvelde, G.H., Ottenhoff, R., van Eijk, M., Aten, J., Kuiper, J., Overkleeft, H.S., Groen, A.K., Verhoeven, A.J. *et al.* (2012) Correction of liver steatosis by a hydrophobic iminosugar modulating glycosphingolipids metabolism. *PLoS One*, **7**, e38520.
56. Bandyopadhyay, U., Nagy, M., Fenton, W.A. and Horwich, A.L. (2014) Absence of lipofuscin in motor neurons of SOD1-linked ALS mice. *Proc. Natl Acad. Sci. USA*, **111**, 11055–11060.
57. Guenther, G.G., Peralta, E.R., Rosales, K.R., Wong, S.Y., Siskind, L.J. and Edinger, A.L. (2008) Ceramide starves cells to death by downregulating nutrient transporter proteins. *Proc. Natl Acad. Sci. USA*, **105**, 17402–17407.
58. Guenther, G.G. and Edinger, A.L. (2009) A new take on ceramide: starving cells by cutting off the nutrient supply. *Cell Cycle*, **8**, 1122–1126.
59. Halter, B., Gonzalez De Aguilar, J.L., Rene, F., Petri, S., Fricker, B., Echaniz-Laguna, A., Dupuis, L., Larmet, Y. and Loeffler, J.P. (2010) Oxidative stress in skeletal muscle stimulates early expression of Rad in a mouse model of amyotrophic lateral sclerosis. *Free Radic. Biol. Med.*, **48**, 915–923.
60. Brooks, B.R., Miller, R.G., Swash, M. and Munsat, T.L., World Federation of Neurology Research Group on Motor Neuron Diseases. (2000) El Escorial revisited: revised criteria for the diagnosis of amyotrophic lateral sclerosis. *Amyotroph. Lateral Scler. Other Motor Neuron Disord.*, **1**, 293–299.
61. Croixmarie, V., Umbdenstock, T., Cloarec, O., Moreau, A., Pascussi, J.M., Boursier-Neyret, C. and Walther, B. (2009) Integrated comparison of drug-related and drug-induced ultra performance liquid chromatography/mass spectrometry metabonomic profiles using human hepatocyte cultures. *Anal. Chem.*, **81**, 6061–6069.
62. Neville, D.C., Coquard, V., Priestman, D.A., te Vruchte, D.J., Sillence, D.J., Dwek, R.A., Platt, F.M. and Butters, T.D. (2004) Analysis of fluorescently labeled glycosphingolipid-derived oligosaccharides following ceramide glycanase digestion and anthranilic acid labeling. *Anal. Biochem.*, **331**, 275–282.
63. Kabashi, E., El Oussini, H., Bercier, V., Gros-Louis, F., Valdmanis, P.N., McDearmid, J., Mejier, I.A., Dion, P.A., Dupre, N., Hollinger, D. *et al.* (2013) Investigating the contribution of VAPB/ALS8 loss of function in amyotrophic lateral sclerosis. *Hum. Mol. Genet.*, **22**, 2350–2360.
64. Werner, E., Croixmarie, V., Umbdenstock, T., Ezan, E., Chaminade, P., Tabet, J.C. and Junot, C. (2008) Mass spectrometry-based metabolomics: accelerating the characterization of discriminating signals by combining statistical correlations and ultrahigh resolution. *Anal. Chem.*, **80**, 4918–4932.